

RECEIVED: October 30, 2023 REVISED: February 7, 2024 ACCEPTED: February 19, 2024 PUBLISHED: March 19, 2024

Four-jet event shapes in hadronic Higgs decays

Aude Gehrmann-De Ridder, a,b Christian T Preussa,c and Ciaran Williamsd

^aInstitute for Theoretical Physics, ETH,

CH-8093 Zürich, Switzerland

^bDepartment of Physics, University of Zürich,

CH-8057 Zürich, Switzerland

^cDepartment of Physics, University of Wuppertal,

42119 Wuppertal, Germany

^dDepartment of Physics, University at Buffalo, The State University of New York, Buffalo 14260, U.S.A.

 $E ext{-}mail:$ gehra@phys.ethz.ch, preuss@uni-wuppertal.de, ciaranwi@buffalo.edu

ABSTRACT: We present next-to-leading order perturbative QCD predictions for four-jet-like event-shape observables in hadronic Higgs decays. To this end, we take into account two Higgs-decay categories: involving either the Yukawa-induced decay to a $b\bar{b}$ pair or the loop-induced decay to two gluons via an effective Higgs-gluon-gluon coupling. We present results for distributions related to the event-shape variables thrust minor, light-hemisphere mass, narrow jet broadening, D-parameter, and Durham four-to-three-jet transition variable. For each of these observables we study the impact of higher-order corrections and compare their size and shape in the two Higgs-decay categories. We find large NLO corrections with a visible shape difference between the two decay modes, leading to a significant shift of the peak in distributions related to the H \rightarrow gg decay mode.

KEYWORDS: Higher-Order Perturbative Calculations, Jets and Jet Substructure, Specific QCD Phenomenology

ARXIV EPRINT: 2310.09354

Contents

Introduction	1
Hadronic Higgs decays up to NLO QCD	2
2.1 General framework	Ę
2.2 Yukawa-induced contributions	(
2.3 Effective-theory contributions	
2.4 Validation	7
Results	8
3.1 Numerical setup and scale-variation prescription	8
3.2 Four-jet event-shape observables	8
3.3 Infrared behaviour	10
3.4 Comparison of predictions in both Higgs-decay categories	10
Conclusions	16
	Hadronic Higgs decays up to NLO QCD 2.1 General framework 2.2 Yukawa-induced contributions 2.3 Effective-theory contributions 2.4 Validation Results 3.1 Numerical setup and scale-variation prescription 3.2 Four-jet event-shape observables 3.3 Infrared behaviour 3.4 Comparison of predictions in both Higgs-decay categories

1 Introduction

Future lepton colliders, such as the FCC-ee [1], the CEPC [2], or the ILC [3], are projected to operate as so-called "Higgs factories", producing an unprecedented amount of events which contain a Higgs boson in the final state. In leptonic collisions, Higgs bosons are predominantly produced via the Higgsstrahlung process $e^+e^- \to ZH$ at low centre-of-mass energies ($\lesssim 450\,\text{GeV}$) and via the vector-boson-fusion process $e^+e^- \to \ell\bar{\ell}H$ at high centre-of-mass energies ($\gtrsim 450\,\text{GeV}$). The clean experimental environment of leptonic collisions, in which contamination from QCD backgrounds such as initial-state radiation and multi-parton interactions is absent, will allow for precise measurements of Higgs-boson properties, such as its branching ratios and total width. In particular, it will become possible to have access to so-far unobserved subleading hadronic decay channels such as the decay to gluons or c-quark pairs, which are currently inaccessible in hadron-collider environments, where only the dominant $H \to b\bar{b}$ decay was observed to date [4, 5].

A well suited class of observables used to probe the structure of QCD radiation are so-called event shapes. Event shapes provide direct access to the geometric properties of hadronic events, while at the same time being amenable to perturbative calculations. As such, they have played a vital role in precision studies of the hadronic $\gamma^*/Z \to q\bar{q}$ decay at LEP, enabling for instance precise determinations of the strong coupling constant [6–11]. It is customary to divide event shapes into three- and four-jet event shapes. We define four-jet event shapes as those observables that are non-zero for topologies with four resolved partons and vanish in the limit of planar three-particle configurations. Historically, experimental

¹We note that this differs from the nomenclature sometimes used in resummed calculations, where these are referred to as three-jet event shapes, representing the number of hard radiators.

measurements at LEP have mostly focused on three-jet event shapes in hadronic γ^*/Z decays, matched by a plethora of theoretical results, such as next-to-next-to-leading order (NNLO) in QCD corrections [12–19], resummation of logarithmically enhanced contributions [20–26], and hadronisation effects [27–31]. Four-jet event shapes, in Z decays on the other hand, have had less attention, despite the fact that they give access to important properties of the strong interactions, such as the quadratic Casimirs [32]. Theoretical calculations of four-jet event shapes have generally achieved NLO accuracy in e⁺e⁻ collisions [33–40]. For most of these, also at least the next-to-leading logarithmic (NLL) contributions are known [41–46].

In hadronic Higgs decays, three-jet-like event shapes such as the thrust and energy-energy correlators have been discussed as discriminators of fermionic and gluonic decay channels [47–50]. In [51], the full set of the six "classical" three-jet-like event-shape observables related to the event-shape variables thrust, C-parameter, heavy-hemisphere mass, narrow and wide jet broadening, and the Durham three-to-two-jet transition variable (called y_{23}) have been calculated at NLO QCD for hadronic Higgs decays. The results obtained for the two Higgs-decay categories were compared. It was shown that for all event shapes the size of NLO corrections were larger in the Hgg category. The distributions related to the three-jet event-shape variable thrust and y_{23} showed the most striking shape differences between Higgs decay categories. It was therefore argued that these event shapes could act as discriminators between the two Higgs-decay categories highlighting where the Hgg category could be enhanced. Recently, a novel method to determine branching ratios in hadronic Higgs decays via fractional energy correlators has been proposed in [52]. To the best of our knowledge, four-jet event shapes have not yet been computed in hadronic Higgs decay processes.

With this paper, we aim at delivering, for the first time, theoretical predictions for four-jet-like event shapes in hadronic Higgs decays including perturbative QCD corrections up to the NLO level. The event-shape distributions computed here are related to the event-shape variables narrow jet broadening, D-parameter, light-hemisphere mass, thrust minor, and the four-to-three-jet transition variable in the Durham algorithm (called y_{34}). It is the purpose of this work to compare the impact of higher-order corrections in terms of size, shape, and perturbative stability of these four-jet-like event-shape distributions.

Furthermore, besides its direct applicability in Higgs phenomenology at lepton colliders, our calculation provides necessary ingredients needed for the NNLO and N³LO calculations of jet observables in three-jet and two-jet final states of hadronic Higgs decays, which are currently only known for decays to b-quarks [53, 54].

The paper is structured as follows. In section 2, we discuss the ingredients of our computation for both Higgs-decay categories up to NLO QCD. Our predictions for the five event-shape distributions are presented in section 3. We summarise our findings and give an outlook on future work in section 4.

2 Hadronic Higgs decays up to NLO QCD

Hadronic Higgs decays proceed via two classes of processes; either involving the decay to a quark-antiquark pair, $H \to q\bar{q}$, or the decay to two gluons, $H \to gg$. Within the scope of this work, we consider a five-flavour scheme and assume all light quarks, including the b-quark, to be massless. In order to allow the Higgs boson to decay to a $b\bar{b}$ pair, we keep a non-vanishing

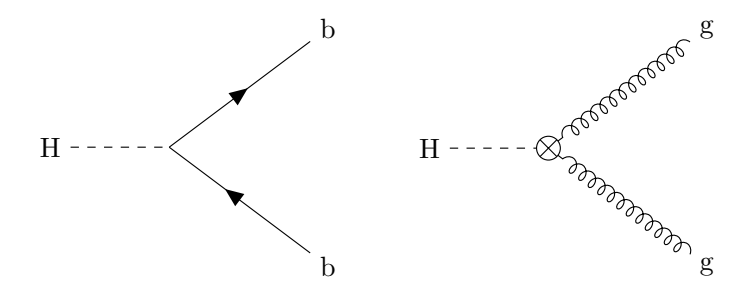


Figure 1. Feynman diagrams of the two decay categories of a Higgs boson decaying into two jets, $H \to b\bar{b}$ (*left*) and $H \to gg$ (*right*).

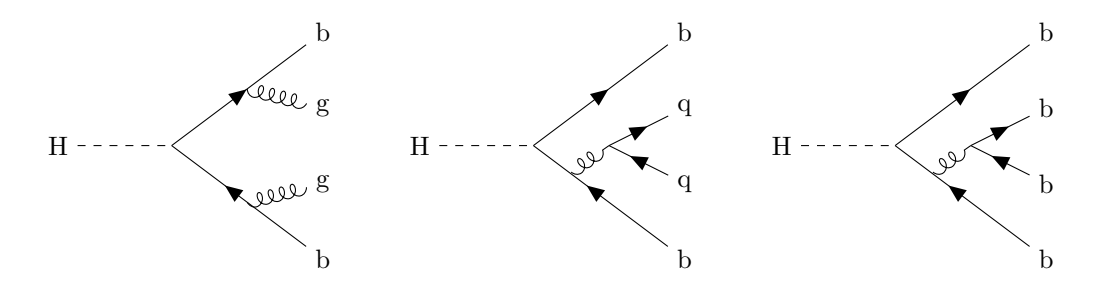


Figure 2. Tree-level Feynman diagrams of four-parton processes in the $H \to b\bar{b}$ decay category contributing to our calculation at LO. Here, q denote any flavour u, d, s, c, b.

Yukawa coupling for the b-quark. The coupling between gluons and the Higgs is considered in an effective theory in the limit of an infinitely heavy top-quark. Based on this, we will classify parton-level processes induced by the two Born-level decay modes into two categories.

In the first class of processes, the Higgs decays to a b-quark pair, mediated by the Yukawa coupling y_b between the Higgs and the bottom quark, and the decay is computed using the Standard-Model Lagrangian. The two-parton decay diagram associated to this decay mode is shown in the left-hand panel of figure 1. In the remainder of this paper, we shall refer to these decay modes as belonging to the Hbb category. The relevant four- and five-parton processes contributing to this decay category, entering our calculation at LO and NLO, respectively, are shown in the first column of table 1. Representative Feynman diagrams for the tree-level four-parton processes contributing at LO are shown in figure 2.

In the second class of processes, the decay proceeds via a top-quark loop. In the limit of an infinitely large top-quark mass, where the top quarks decouple, we compute these decays in an effective theory with a direct coupling of the Higgs field to the gluon field-strength tensor. In this second category, which we shall refer to as the Hgg category, the interaction is mediated by an effective Hgg vertex, which is represented as a crossed dot in the two-parton decay diagram shown in the right-hand part of figure 1. A summary of the four- and five-parton processes contributing to this decay category, entering our computation at LO and NLO, are presented in the second column of table 1. Feynman diagrams for the tree-level four-parton processes contributing at LO are shown in figure 3.

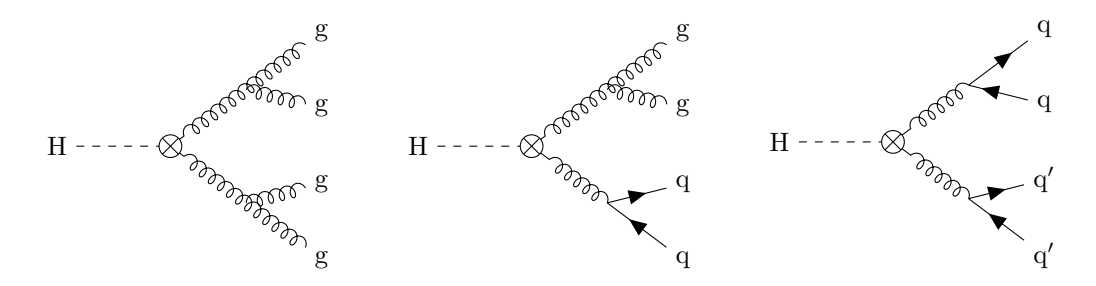


Figure 3. Tree-level Feynman diagrams of four-parton processes in the $H \to gg$ decay category contributing to our calculation at LO. Here, q and q' denote any flavour u, d, s, c, b, possibly with q' = q but $q' \neq q$ in general.

	$\mathrm{H} \to \mathrm{b}\bar{\mathrm{b}}$ type	$H \to gg type$	
LO		$\mathrm{H} o \mathrm{gggg}$	tree-level
	$\mathrm{H} ightarrow \mathrm{bar{b}gg}$	$H \to q\bar{q}gg$	tree-level
	${ m H} ightarrow { m b} { m b} { m q} { m ar q}$	$H \to q\bar q q'\bar q'$	tree-level
	${ m H} ightarrow { m b} { m b} { m b} { m b}$	$H \to q\bar q q\bar q$	tree-level
NLO		$\mathrm{H} o \mathrm{gggg}$	one-loop
	$\mathrm{H} \to \mathrm{b} \bar{\mathrm{b}} \mathrm{g} \mathrm{g}$	$H \to q\bar{q}gg$	one-loop
	$\mathrm{H} ightarrow \mathrm{b} \mathrm{ar{b}} \mathrm{q} \mathrm{ar{q}}$	$H \to q\bar q q'\bar q'$	one-loop
	${ m H} ightarrow { m b} { m b} { m b} { m b}$	$H \to q\bar q q\bar q$	one-loop
		$\mathrm{H} \to \mathrm{ggggg}$	tree-level
	$\mathrm{H} \to \mathrm{bar{b}ggg}$	$H \to q\bar{q}ggg$	tree-level
	$\mathrm{H} ightarrow \mathrm{b} \mathrm{ar{b}} \mathrm{q} \mathrm{ar{q}} \mathrm{g}$	$H \to q\bar q q'\bar q' g$	tree-level
	$\mathrm{H} ightarrow \mathrm{b} \mathrm{ar{b}} \mathrm{b} \mathrm{ar{b}} \mathrm{g}$	$H \to q\bar q q\bar q g$	tree-level

Table 1. Partonic channels contributing to the decay $H \rightarrow 4j$ at LO and NLO.

Following the nomenclature presented in [51], the preceding discussion can be cast into an effective Lagrangian containing both decay categories as,

$$\mathcal{L}_{\text{Higgs}} = -\frac{\lambda(M_{\text{t}}, \mu_{\text{R}})}{4} H G_{\mu\nu}^{a} G^{a,\mu\nu} + \frac{y_{\text{b}}(\mu_{\text{R}})}{\sqrt{2}} H \bar{\psi}_{\text{b}} \psi_{\text{b}}.$$
(2.1)

Here, the effective Higgs-gluon-gluon coupling proportional to $\alpha_{\rm s}$ is given by

$$\lambda(M_{\rm t}, \mu_{\rm R}) = -\frac{\alpha_{\rm s}(\mu_{\rm R})C(M_{\rm t}, \mu_{\rm R})}{3\pi v}, \qquad (2.2)$$

where we define the Higgs vacuum expectation value v and the top-quark Wilson coefficient $C(M_t, \mu_R)$. The b-quark Yukawa coupling on the other hand is given by

$$y_{\rm b}(\mu_{\rm R}) = \frac{4\pi\alpha}{\sqrt{2}M_{\rm W}\sin\theta_{\rm W}} \overline{m}_{\rm b}(\mu_{\rm R}), \qquad (2.3)$$

and depends directly on the b-quark mass. As indicated by the renormalisation-scale dependence, both, the effective Hgg coupling and the Hb $\bar{\rm b}$ Yukawa coupling, are subject to renormalisation, which we here perform in the $\overline{\rm MS}$ scheme with $N_{\rm F}=5$. While the top-quark

Wilson coefficient $C(M_t, \mu_R)$ is known up to $\mathcal{O}(\alpha_s^4)$ in the literature [55–61] we here only need to consider the first-order expansion of the Wilson coefficient $C(M_t, \mu_R)$ in α_s . It is given by

$$C(M_{\rm t}, \mu_{\rm R}) = 1 + \frac{11}{6} N_{\rm C} \frac{\alpha_{\rm s}(\mu_{\rm R})}{2\pi} + \mathcal{O}(\alpha_{\rm s}^2).$$
 (2.4)

which is independent of the top-quark mass M_t . Further, the Yukawa mass \bar{m}_b runs with μ_R , with the running of the Yukawa coupling y_b with μ_R taken into account via the results of [62].

Finally, to conclude some general remarks, we wish to highlight the importance for the present study that the kinematical mass of the b-quark be vanishing. For kinematically massless b-quarks, the operators in the effective Lagrangian given in eq. (2.1) do not interfere or mix under renormalisation, cf. e.g. [48]. In particular, this means that the product of Yukawa-induced amplitudes with HEFT-induced amplitudes vanishes to all orders in α_s when computing squared matrix elements. Moreover, it implies that the Wilson coefficient $C(M_t, \mu_R)$ in eq. (2.4) and the Yukawa coupling $y_b(\mu_R)$ in eq. (2.3) evolve independently under the renormalisation group. As a result, it is possible to consider two distinct decay categories, $H \to b\bar{b}$ and $H \to gg$, and calculate theoretical predictions and higher-order corrections for each of them separately, as done previously in [51] for the case of three-jet-like event shapes. The effect of interferences between the Yukawa-induced decay $H \to b\bar{b}$ and the HEFT-induced $H \to gg$ to order $\mathcal{O}(\alpha_s^3)$ in a framework with massive b-quarks and c-quarks has been studied in [63].

In the remainder of this section we discuss in detail the ingredients of our computation. We split the discussion in the following parts. In section 2.1, we present the general framework enabling us to compute Higgs-decay observables up to NLO, while in section 2.2 and section 2.3 we discuss details of the ingredients and their numerical implementation in the two Higgs-decay categories. In section 2.4, we provide a summary of the checks performed to validate our results.

2.1 General framework

Given an infrared-safe observable O, the differential four-jet decay rate of a colour-singlet resonance of mass M, like the Standard-Model scalar Higgs boson, can be written at each perturbative order up to NLO level (i.e., including corrections up to the third order in the strong coupling α_s) as

$$\frac{1}{\Gamma^{(n)}(\mu_{\rm R})} \frac{\mathrm{d}\Gamma}{\mathrm{d}O}(\mu_{\rm R}, O) = \left(\frac{\alpha_{\rm s}(\mu_{\rm R}^2)}{2\pi}\right)^2 \frac{\mathrm{d}\bar{B}}{\mathrm{d}O} + \left(\frac{\alpha_{\rm s}(\mu_{\rm R}^2)}{2\pi}\right)^3 \left(\frac{\mathrm{d}\bar{C}}{\mathrm{d}O} + \beta_0 \log\left(\frac{\mu_{\rm R}^2}{M^2}\right) \frac{\mathrm{d}\bar{B}}{\mathrm{d}O}\right), \quad (2.5)$$

where $d\bar{B}$ and $d\bar{C}$ denote the differential LO and NLO coefficients, respectively. Subject to the order of the calculation, n, the differential decay rate in eq. (2.5) is normalised to the LO (n=0) or NLO (n=1) partial width, $\Gamma^{(1)}$ or $\Gamma^{(0)}$, respectively.

Schematically, the LO coefficient B can be determined as

$$\left(\frac{\alpha_{\rm s}}{2\pi}\right)^2 \frac{\mathrm{d}\bar{B}}{\mathrm{d}O} = \frac{1}{\Gamma^{(n)}} \int \frac{\mathrm{d}\Gamma^{\rm B}}{\mathrm{d}\Phi_4} \delta(O - O(\Phi_4)) \,\mathrm{d}\Phi_4 \,, \tag{2.6}$$

while the NLO coefficient C is obtained as

$$\left(\frac{\alpha_{\rm s}}{2\pi}\right)^3 \frac{\mathrm{d}\bar{C}}{\mathrm{d}O} = \frac{1}{\Gamma^{(n)}} \int \left[\frac{\mathrm{d}\Gamma^{\rm V}}{\mathrm{d}\Phi_4} + \frac{\mathrm{d}\Gamma^{\rm T}_{\rm NLO}}{\mathrm{d}\Phi_4}\right] \delta(O - O(\Phi_4)) \,\mathrm{d}\Phi_4 \tag{2.7}$$

$$+ \frac{1}{\Gamma^{(n)}} \int \left[\frac{\mathrm{d}\Gamma^{\mathrm{R}}}{\mathrm{d}\Phi_{5}} \delta(O - O(\Phi_{5})) - \frac{\mathrm{d}\Gamma^{\mathrm{S}}_{\mathrm{NLO}}}{\mathrm{d}\Phi_{5}} \delta(O - O(\Phi_{4}(\Phi_{5}))) \right] d\Phi_{5}. \tag{2.8}$$

Here, $d\Gamma^R$ and $d\Gamma^V$ denote the real and virtual (one-loop) correction differential in the fourparton and five-parton phase space, respectively. The real and virtual subtraction terms $d\Gamma^S_{NLO}$ and $d\Gamma^T_{NLO}$, on the other hand, ensure that the real and virtual corrections are separately infrared finite and make them amenable to numerical integration. The notation $\Phi_4(\Phi_5)$ represents a kinematic mapping from the five-parton to the four-parton phase space, specific to the subtraction term $d\Gamma^S_{NLO}$. The choice of subtraction terms is in principle arbitrary and subject only to the requirements that the virtual subtraction term $d\Gamma^T_{NLO}$ cancels all explicit poles in $d\Gamma^V$, the real subtraction term $d\Gamma^S_{NLO}$ cancels all implicit singularities in $d\Gamma^R$, and the net contribution of the subtraction terms to the decay width vanishes,

$$\int \frac{d\Gamma_{\text{NLO}}^{\text{T}}}{d\Phi_4} d\Phi_4 = \int \frac{d\Gamma_{\text{NLO}}^{\text{S}}}{d\Phi_5} d\Phi_5.$$
 (2.9)

The last requirement is equivalent to demanding that $d\Gamma_{\rm NLO}^{\rm T}$ be the integral of $d\Gamma_{\rm NLO}^{\rm S}$ over the respective one-particle branching phase space. To compute our predictions for the four-jet like hadronic event shapes in Higgs decays, we here rely on the antenna-subtraction framework [40, 64, 65] to construct all subtraction terms and implement our calculation in the publicly available² EERAD3 framework [14]. This code has previously been used to study event shapes [12, 13] and jet distributions [66] in $e^+e^- \to 3j$ at NNLO and was recently extended to include hadronic Higgs decays to three jets at NLO [51]. Our new implementation builds upon the latter and is done in a flexible manner, utilising the existing infrastructure, such as phase-space generators of the $e^+e^- \to 3j$ calculation at NNLO. In particular, the real-radiation contributions proportional to α_s^2 of the three-jet computation of Higgs-decay observables enter our current calculation of four-jet-like observables at the Born level. We implement all matrix elements and subtraction terms in analytic form, enabling a fast and numerically stable evaluation of the perturbative coefficients up to NLO level.

2.2 Yukawa-induced contributions

Four-particle tree-level matrix elements in the Hb $\bar{\rm b}$ category are taken from the NLO H \to b $\bar{\rm b}j$ process in [51], which have been calculated explicitly using FORM [67]. Tree-level five-parton matrix elements are taken from the N³LO H \to b $\bar{\rm b}$ and NNLO H \to b $\bar{\rm b}j$ calculation in [53, 54], in turn calculated using BCFW recursion relations [68]. Similarly, one-loop four-parton amplitudes are taken from the same calculation [53, 54]. These have been derived analytically by use of the generalised unitarity approach [69], using quadruple cuts for box coefficients [70], triple cuts for triangle coefficients [71], double cuts for bubble coefficients [72], and d-dimensional unitarity techniques for the rational pieces [73].

²http://eerad3.hepforge.org.

As per eq. (2.5), the differential four-jet rate depends on the partial two-parton width. At NLO, the inclusive width of the H \rightarrow b $\bar{\rm b}$ decay reads

$$\Gamma_{\rm H\to b\bar{b}}^{(1)}(\mu_{\rm R}) = \left[1 + \left(\frac{\alpha_{\rm s}(\mu_{\rm R}^2)}{2\pi} \right) \left(\frac{17}{2} C_{\rm F} + 3C_{\rm F} \log \left(\frac{\mu_{\rm R}^2}{M_{\rm H}^2} \right) \right) \right] \Gamma_{\rm H\to b\bar{b}}^{(0)}(\mu_{\rm R}) , \qquad (2.10)$$

where the LO partial width is given by

$$\Gamma_{\rm H \to b\bar{b}}^{(0)}(\mu_{\rm R}) = \frac{y_{\rm b}^2(\mu_{\rm R})M_{\rm H}N_{\rm C}}{8\pi} \,.$$
(2.11)

The running of the Yukawa coupling y_b with μ_R present in the partial width is taken into account via the results of [62].

2.3 Effective-theory contributions

In the Hgg category, we take the four-parton tree-level matrix elements from the NLO H \rightarrow 3j calculation in the Hgg category presented in [51]. Five-parton tree-level and four-parton one-loop amplitudes are obtained by crossing the ones used in the $pp \rightarrow H + 1j$ NNLO calculation in NNLOJET [74, 75]. The five-parton tree-level amplitudes are based on the results presented in [76–79], while the four-parton one-loop amplitudes are based on the results presented in [76, 79–86]. The four-parton decay rate further receives contributions from the $\mathcal{O}(\alpha_s)$ expansion of the top-quark Wilson coefficient $C(M_t, \mu_R)$. We implement these as a finite contribution to the virtual correction,

$$d\Gamma^{V} \to d\Gamma^{V} + \left(\frac{\alpha_{s}}{2\pi}\right) \frac{11}{3} N_{C} d\Gamma^{B}$$
 (2.12)

As per eq. (2.5), the differential four-jet rate depends on the partial two-parton width. At NLO, the inclusive width of the H \rightarrow gg decay reads

$$\Gamma_{\rm H\to gg}^{(1)}(\mu_{\rm R}) = \left[1 + \left(\frac{\alpha_{\rm s}(\mu_{\rm R}^2)}{2\pi} \right) \left(\frac{95}{6} C_{\rm A} - \frac{7}{3} N_{\rm F} + 2\beta_0 \log \left(\frac{\mu_{\rm R}^2}{M_{\rm H}^2} \right) \right) \right] \Gamma_{\rm H\to gg}^{(0)}(\mu_{\rm R}) , \qquad (2.13)$$

where the LO partial width is given by

$$\Gamma_{\rm H\to gg}^{(0)}(\mu_{\rm R}) = \frac{\alpha_{\rm s}^2(\mu_{\rm R})G_{\rm F}M_{\rm H}^3}{36\pi^2\sqrt{2}}.$$
(2.14)

2.4 Validation

We have performed numerical checks of all matrix elements on a point-by-point basis against automated tools. Tree-level four- and five-parton matrix elements are tested against results generated with MADGRAPH5 [87, 88], whereas four-parton one-loop matrix elements are validated using OPENLOOPS 2 [89]. In all cases, we have found excellent agreement between our analytic expressions and the auto-generated results.

Real subtraction terms $d\Gamma_{\rm NLO}^{\rm S}$ have been tested numerically using so-called "spike tests", first introduced in the context of the antenna-subtraction framework in [90] and applied to the NNLO di-jet calculation in [91]. To this end, trajectories into singular limits are generated using Rambo [92] and the ratio $d\Gamma_{\rm NLO}^{\rm S}/d\Gamma^{\rm R}$ is evaluated on a point-by-point basis.

Where applicable, azimuthal correlations are included via summation over antipodal points. In all relevant single-unresolved limits, we have found very good agreement between the subtraction terms and real-radiation matrix elements.

To confirm the cancellation of explicit poles in the virtual corrections $d\Gamma^{V}$ by the virtual subtraction terms $d\Gamma^{T}_{NLO}$, we have both checked the cancellation analytically and numerically.

3 Results

In the following, we shall present numerical results for the five different four-jet event shapes: thrust minor, light-hemisphere mass, narrow jet broadening, D-parameter, and the four-to-three-jet transition variable in the Durham algorithm. We discuss our numerical setup and scale-variation prescription in section 3.1, before defining the four-jet event-shape observables in section 3.2. Theoretical predictions are shown and discussed in section 3.4.

3.1 Numerical setup and scale-variation prescription

We consider on-shell Higgs decays with a Higgs mass of $M_{\rm H}=125.09\,{\rm GeV}$. We work in the G_{μ} -scheme and consider electroweak quantities as constant parameters. Specifically, we consider the following electroweak input parameters

$$G_{\rm F} = 1.20495 \times 10^{-5} \,\text{GeV}^{-2} \,, \quad M_{\rm Z} = 91.1876 \,\text{GeV} \,, \quad M_{\rm W} = 80.385 \,\text{GeV} \,, \quad (3.1)$$

yielding a corresponding value of $\alpha = \frac{1}{128}$. As alluded to above, we keep a vanishing kinematical mass of the b-quark throughout the calculation, but consider a non-vanishing Yukawa mass. The running of the Yukawa mass with $\mu_{\rm R}$ is calculated using the results of [62], corresponding to $\bar{m}_{\rm b}(M_{\rm H})$ close to 2.61 GeV.

We choose the Higgs mass as renormalisation scale, $\mu_{\rm R}=M_{\rm H}$, and apply a scale variation $\mu_{\rm R}\to k_\mu\mu_{\rm R}$ about this central scale with $k_\mu\in\left[\frac{1}{2},2\right]$. We wish to point out that this prescription also affects the normalisation of our distributions via eq. (2.5). We use one-and two-loop running for the strong coupling $\alpha_{\rm s}$, at LO and NLO respectively, obtained by solving the renormalisation-group equation at the given order, as detailed in [12, 14]. For the strong coupling, we choose a nominal value at scale $M_{\rm Z}$ given by

$$\alpha_{\rm s}(M_{\rm Z}) = 0.1179\,, ag{3.2}$$

corresponding to the current world average [93].

3.2 Four-jet event-shape observables

We consider the five different four-jet event-shape observables related to the following event shapes thrust minor, light-hemisphere mass, narrow jet broadening, D-parameter, and the Durham four-to-three-jet transition variable. They are defined as follows [40]:

Thrust minor. We define thrust minor as

$$T = \left(\frac{\sum_{j} |\vec{p}_{j} \cdot \vec{n}_{\text{Min}}|}{\sum_{k} |\vec{p}_{k}|}\right), \tag{3.3}$$

where \vec{n}_{Min} is given by $\vec{n}_{\text{Min}} = \vec{n}_{\text{T}} \times \vec{n}_{\text{Maj}}$. Here, \vec{n}_{T} is the thrust axis [94, 95], defined as the unit vector which maximises

$$T = \max_{\vec{n}} \left(\frac{\sum_{j} |\vec{p}_j \cdot \vec{n}|}{\sum_{k} |\vec{p}_k|} \right) , \tag{3.4}$$

and \vec{n}_{Maj} is a unit vector for which in addition $\vec{n}_{\text{Maj}} \cdot \vec{n}_{\text{T}} = 0$ holds. The thrust minor measures the distribution of particles orthogonal to the plane defined by \vec{n}_{T} and \vec{n}_{Maj} . It vanishes for topologies with less than four particles, as three particles always span a plane parallel to the thrust and thrust-major axis and two particles exactly align with the thrust axis.

Light-hemisphere mass. Starting from the thrust axis $\vec{n}_{\rm T}$, events are divided into two hemispheres (jets), H_1 and H_2 , separated by an axis orthogonal to $\vec{n}_{\rm T}$. For each hemisphere, the hemisphere mass is calculated as

$$\frac{M_i^2}{s} = \frac{1}{E_{\text{vis}}^2} \left(\sum_{j \in H_1} p_j \right)^2, \tag{3.5}$$

with E_{vis} the visible energy in the event. The light hemisphere mass is then given by the smaller of the two hemisphere masses [96],

$$\frac{M_{\rm L}^2}{s} = \min_{i \in \{1,2\}} \left(\frac{M_i^2}{s}\right). \tag{3.6}$$

For massless particles, the light-hemisphere mass is non-vanishing only for topologies with at least four particles, as the lighter hemisphere will otherwise always consist of a single particle.

Narrow jet broadening. Jet broadenings measure the distribution of the transverse momenta of particles with respect to the thrust axis. The narrow jet broadening is defined as the jet-broadening value of the more narrow hemisphere,

$$B_{\rm N} = \min(B_1, B_2),$$
 (3.7)

with the hemisphere broadenings B_i given by [97]

$$B_{i} = \frac{\sum_{j \in H_{i}} |\vec{p}_{j} \times \vec{n}_{T}|}{2 \sum_{k} |\vec{p}_{k}|},$$
(3.8)

for the two hemispheres H_1 and H_2 defined by the thrust axis. Since a single particle has a vanishing hemisphere broadening, the narrow jet broadening is zero for events with less than four particles, for which always one of the hemispheres contains only a single particle.

D-parameter. The *D*-parameter measures the planarity of an event and vanishes for planar configurations. As such, it is non-zero only for events containing at least four particles, as three (or less) particles always span a plane. It is defined as [35]

$$D = 27\lambda_1\lambda_2\lambda_3\,, (3.9)$$

given in terms of the three eigenvalues λ_1 , λ_2 , and λ_3 of the linearised momentum tensor,

$$\Theta^{\alpha\beta} = \frac{1}{\sum_{k} |\vec{p}_k|} \sum_{j} \frac{p_j^{\alpha} p_j^{\beta}}{|\vec{p}_j|}, \text{ with } \alpha, \beta \in \{1, 2, 3\}.$$

$$(3.10)$$

Four-to-three-jet transition variable. The four-to-three-jet transition variable denoted by y_{34} corresponds to the jet resolution parameter y_{cut} at which an event changes from a four-jet to a three-jet event according a specific clustering algorithm. Here, we specifically consider the Durham algorithm, in which the distance measure reads

$$y_{ij}^{D} = \frac{2E_i E_j (1 - \cos \theta_{ij})}{E_{\text{vis}}^2} \,. \tag{3.11}$$

We use the so-called E-scheme, in which the four-momenta of the two particles are added linearly in each step of the algorithm,

$$p_{ij} = p_i + p_j \,. (3.12)$$

3.3 Infrared behaviour

All observables introduced in section 3.2 are non-vanishing only for at least four resolved particles. In the region of phase space where only three jets can be resolved, i.e., where the observables of section 3.2 become small, the differential rate becomes enhanced by large logarithms of the form $\log^m(1/O)$. In this phase-space region, fixed-order calculations become unreliable and a faithful calculation of the differential decay width requires the resummation of the large logarithms.

To avoid large logarithmic contributions spoiling the convergence of our fixed-order calculation in the three-jet region, we restrict the range of validity of our predictions as follows: we impose a small cut-off $y_0 = 10^{-5}$ on linear distributions and $y_0 = e^{-7}$ on logarithmically binned distributions. We consider this minimal value for all observables mentioned above in section 3.2 with the exception of the distribution related to the four-to-three-jet transition variable y_{34} , where we require a cut off at $y_0 = e^{-10}$. The y_0 cut-offs are imposed on both four- and five-parton configurations and ensure the reliability of our predictions in the whole kinematical region considered.

In addition to the observable cutoff y_0 , we introduce a technical cut-off t_{cut} and require that all dimensionless two-parton invariants in the five-parton states to be above this cut, $s_{ij}/s > t_{\text{cut}}$. This technical cut-off parameter improves the numerical stability of the antenna-subtraction procedure by avoiding large numerical cancellations between the real subtraction term and the real matrix element. By default, we employ a technical cut-off of $t_{\text{cut}} = 10^{-7}$.

We note that there is a subtle interplay of the observable cut-off y_0 and the technical cut-off t_{cut} . We have studied this interplay for all observables considered in section 3.2 by varying the technical cut-off between $t_{\text{cut}} \in \{10^{-8}, 10^{-7}, 10^{-6}\}$ and verified that this variation leaves all distributions above the observable cut-off y_0 unaffected. We further wish to emphasise that the independence on t_{cut} also validates the correct implementation of our subtraction terms.

3.4 Comparison of predictions in both Higgs-decay categories

In this subsection, we present theoretical predictions at LO and NLO QCD for the event shapes defined in section 3.2. For each event shape, we show two binnings in the observable; a linear binning to highlight the general structure and a logarithmic binning to emphasise the behaviour of the distribution in the infrared region, in particular the position of its peak.

In all cases, we present results according to eq. (2.5). In particular, we normalise by the LO (NLO) partial two-jet decay width for LO (NLO) distributions.³

Numerical predictions for the five event-shape observables are shown in figures 4, 5, 6, 7 and 8. Each figure contains four plots; we present results with linear binning in the top row and results with logarithmic binning in the bottom row; results in the $H \to b\bar{b}$ decay category are shown in the left-hand column, while results in the $H \to gg$ decay category are shown in the right-hand column. Each plot contains LO and NLO predictions, shown with a dashed and solid line, respectively. Predictions obtained by the scale variation are shown with lighter shading. The infrared region is located towards the left-hand side of each plot, whereas the hard multi-particle region is located on the right-hand side.

All distributions exhibit the usual characteristics of event-shape observables at fixed order. The LO distributions diverge towards positive infinity in the infrared limit on the left-hand side of the plots. In these regions of phase space, one of the four particles in the LO Born configuration becomes unresolved and the four-particle configuration assumes the shape of a planar three-jet event. At NLO, the distributions develop a peak close to zero and diverge towards negative infinity in the infrared limit. As a consequence, all distributions show these characteristic behaviour towards the infrared region. As mentioned before, an accurate description of the observables in this phase-space region requires the resummation of large logarithms, which we do not include in our predictions. Instead as detailed in section 3.3, we restrict ourselves to provide predictions above a minimum value of the observables. Generically, we observe rather large NLO corrections with K-factors between 1.3 and 2.3 and scale uncertainties of similar size in both categories. It may be surprising that these corrections are numerically slightly bigger for the $H \to bb$ decay category. The reason for this is an interplay of two effects. On the one hand, predictions in the Hgg category generally receive larger NLO corrections, which results in numerically bigger NLO coefficients dC/dO. On the other hand, the NLO distribution are normalised by $1/\Gamma^{(1)}$, as opposed to $1/\Gamma^{(0)}$ in the LO case, cf. eq. (2.5). Because the NLO correction to the partial two-particle decay width is again numerically bigger for $H \to gg$ decays than for $H \to bb$ decays (~ 1.6 compared to ~ 1.2 at $\mu_{\rm R} = M_{\rm H}$), the NLO distributions are subject to a more sizeable scaling. For the observables considered here, this has the effect that the full NLO correction becomes numerically smaller in the $H \to gg$ decay category.

Thrust minor. In figure 4 we present results for the thrust minor at LO and NLO in the two decay categories. In both decay modes, we observe rather large NLO corrections, with K-factors at the central scale around 1.9 in the Hb $\bar{\rm b}$ category and 1.7 in the Hgg category. In addition, there is a visible shape difference between the two decay modes, as can be inferred from the plots in the top row (with linear binning) of figure 4. We observe a substantial shift of the peak of the Hgg distribution away from the infrared region on the left-hand side of the plots. Further, the Hb $\bar{\rm b}$ NLO correction follows a rather flat shape, while the Hgg NLO correction has a more curved shape, as can be seen in the ratio panels of the top-row plots. This assessment is confirmed by the logarithmically binned distributions shown in the bottom row of figure 4. From the ratio panels in the bottom-row plots, it is visible that the

 $^{^{3}}$ We refrain from reweighting by the branching ratios of the Hb $\overline{\rm b}$ and Hgg decays as done in [51].

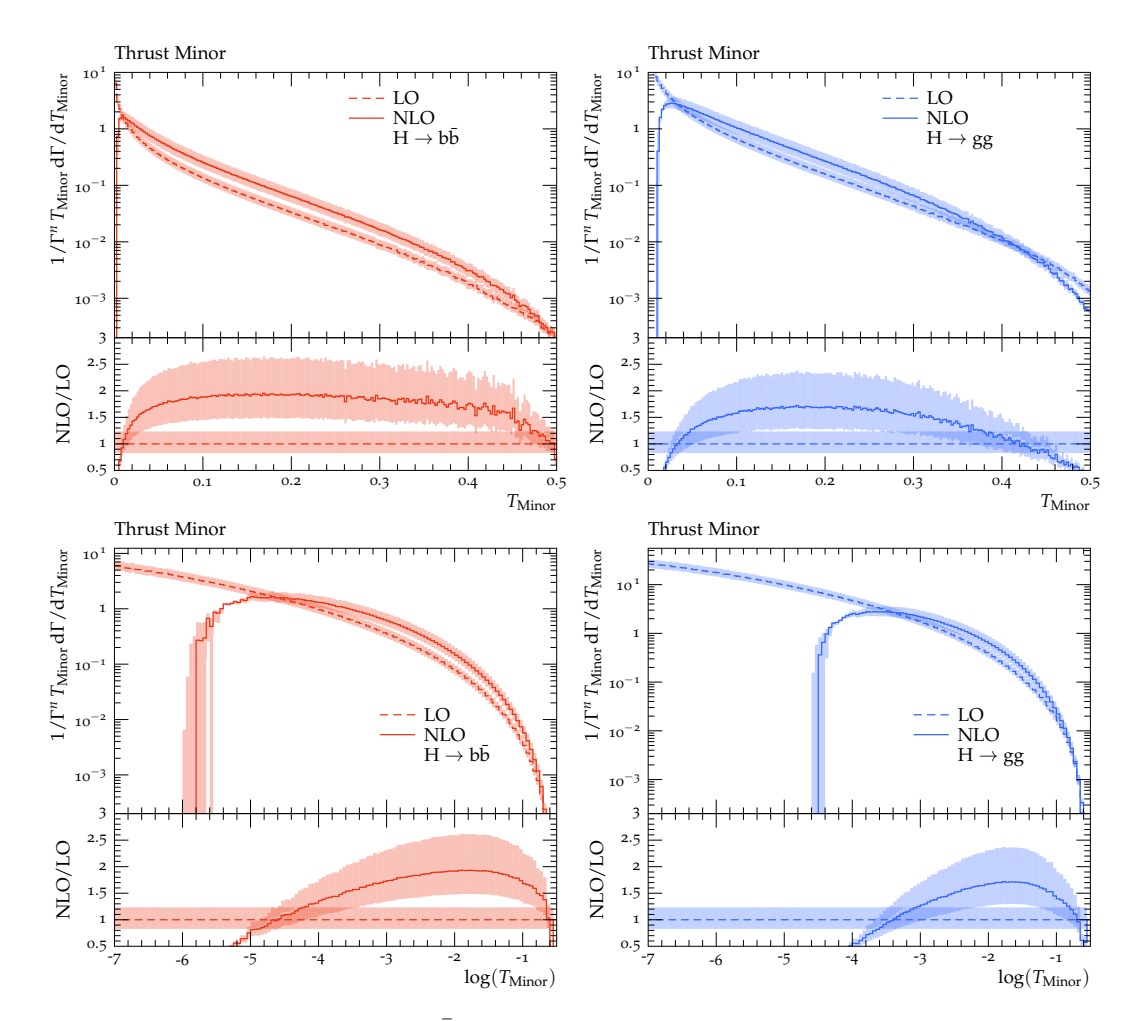


Figure 4. Thrust minor in the $H \to b\bar{b}$ (*left*) and $H \to gg$ (*right*) decay category. The top row shows linearly binned histograms, the bottom row shows the same histograms with logarithmic binning, see main text.

intersection of the LO and NLO predictions is located at $\log(T_{\rm Minor}) = -4.6$ in the H \rightarrow bb case and at $\log(T_{\rm Minor}) = -3.4$ in the H \rightarrow gg case.

Light-hemishere mass. In figure 5, LO and NLO results for the light-hemisphere mass in the two decay categories are shown. From the top row of the figure, with linear binning, it is evident that the peak of the NLO distributions is located further in the infrared region in both Higgs-decay categories. It cannot be fully resolved in the Hb $\bar{\rm b}$ category but only in the Hgg category. This is confirmed by the bottom row of figure 5, which shows that the intersection of the LO and NLO predictions is located at $\log(M_{\rm L}^2/s) < -7$ in the Hb $\bar{\rm b}$ category and at $\log(M_{\rm L}^2/s) = -5$ in the Hgg category. This manifests itself in a shift of the peak of the H \rightarrow gg distribution towards harder scales with respect to the peak of the H \rightarrow b $\bar{\rm b}$ distribution, as can be best seen in the plots in the top row of figure 5. From the ratio plots, we see that the NLO corrections are again rather large, with values at the central scale of about 2.0 in the H \rightarrow b $\bar{\rm b}$ category and 1.6 in the H \rightarrow gg category. Generally, the shape of the NLO correction is rather similar, being mostly flat for the two decay categories.

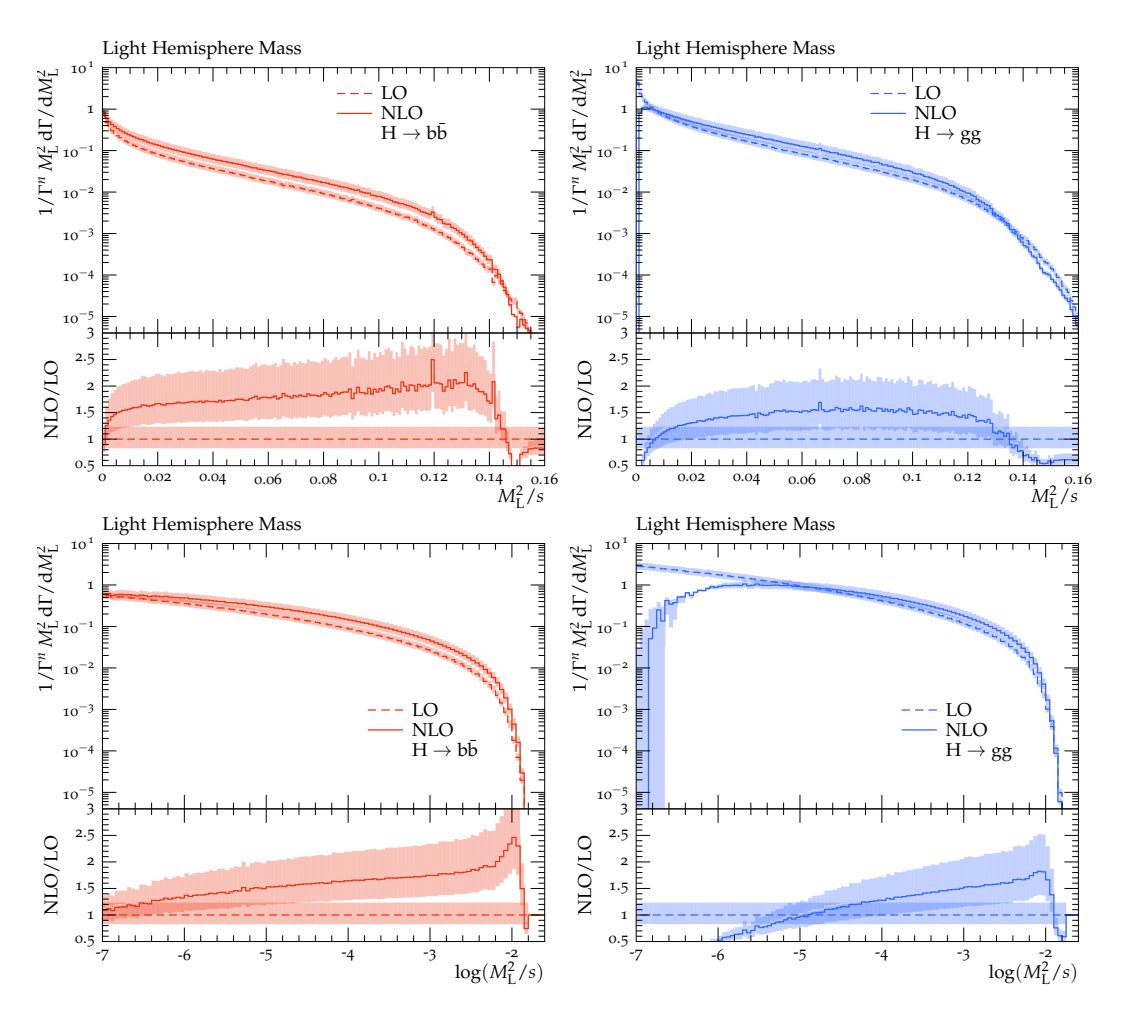


Figure 5. Light hemisphere mass in the $H \to b\bar{b}$ (*left*) and $H \to gg$ (*right*) decay category. The top row shows linearly binned histograms, the bottom row shows the same histograms with logarithmic binning, see main text.

Narrow jet broadening. Figure 6 shows results for the narrow jet broadening in both decay categories at LO and NLO. In both decay categories, the peak of the NLO distributions as well as its shift away from the planar three-jet limit in the Hgg case is clearly visible in the top-row plots. The bottom row of figure 6 shows that the intersection of the LO and NLO distributions is located at $\log(B_{\rm Min}) = -5.5$ in the Hbb decay category, while it is shifted to a significantly larger value of $\log(B_{\rm Min}) = -3.7$ in the Hgg decay category. The shape of the NLO corrections at the central scale is rather flat around a factor of 1.8 for Hbb decays, but slightly curved at around 1.4 in Hgg decays.

D-parameter. In figure 7 we present LO and NLO results for the *D*-parameter in the two decay categories. We observe large NLO corrections with K-factors at the central scale of 2.3 in the Hb $\bar{\rm b}$ decay and 1.8 in the Hgg decay. The shape of the NLO corrections is comparable to thrust minor, as can be seen from comparing the ratio panels in the top row of figure 7 with the ones in the top row of figure 4. Most notably, the shape of NLO

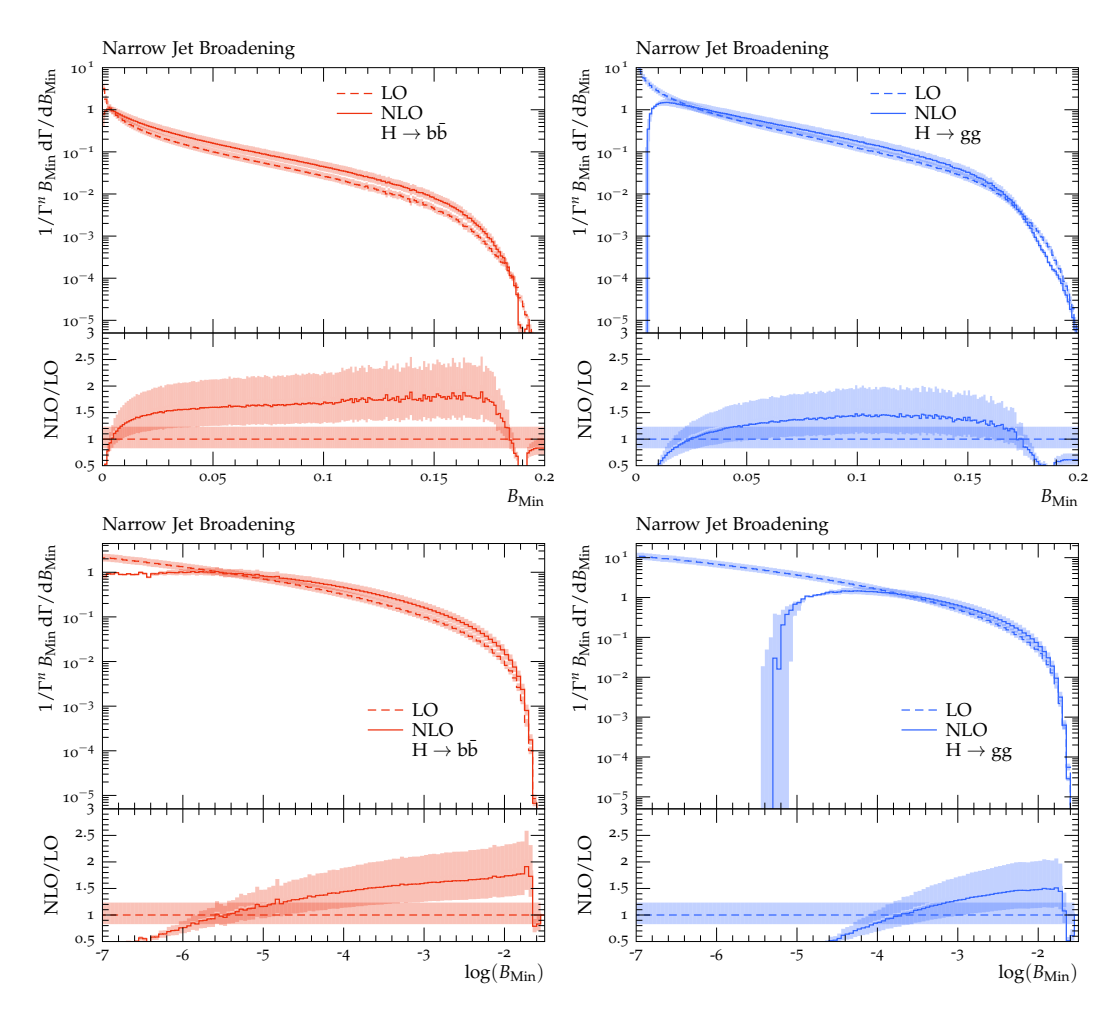


Figure 6. Narrow jet broadening in the $H \to b\bar{b}$ (*left*) and $H \to gg$ (*right*) decay category. The top row shows linearly binned histograms, the bottom row shows the same histograms with logarithmic binning, see main text.

corrections is rather flat for Hb $\bar{\rm b}$ decays, while it is more curved for Hgg decays. The ratio panels in the logarithmically binned distributions in the bottom row of figure 7 reveal the location of the LO-NLO intersection. Specifically, it sits at $\log(D) = -5.6$ for Hb $\bar{\rm b}$ decays and $\log(D) = -4.2$ for Hgg decays.

Four-to-three-jet transition variable. Figure 8 contains results for the four-to-three-jet transition variable denoted by y_{34} , using the Durham jet algorithm to build jets at LO and NLO for the two decay categories. We note that, different to the other event shapes, we plot results for this four-jet resolution distribution only with a logarithmic binning. Nevertheless, we observe similar results as before. Events in the Hgg category are generally clustered earlier and the intersection of the LO and NLO curves is shifted by about two orders of magnitude away from the infrared limit, from $\log(y_{34}) = -8.1$ in the Hbb case to $\log(y_{34}) = -5.6$ in the Hgg case. The NLO corrections are rather mild, with K-factors at the central scale around 1.7 for Hbb decays and 1.3 for Hgg decays.

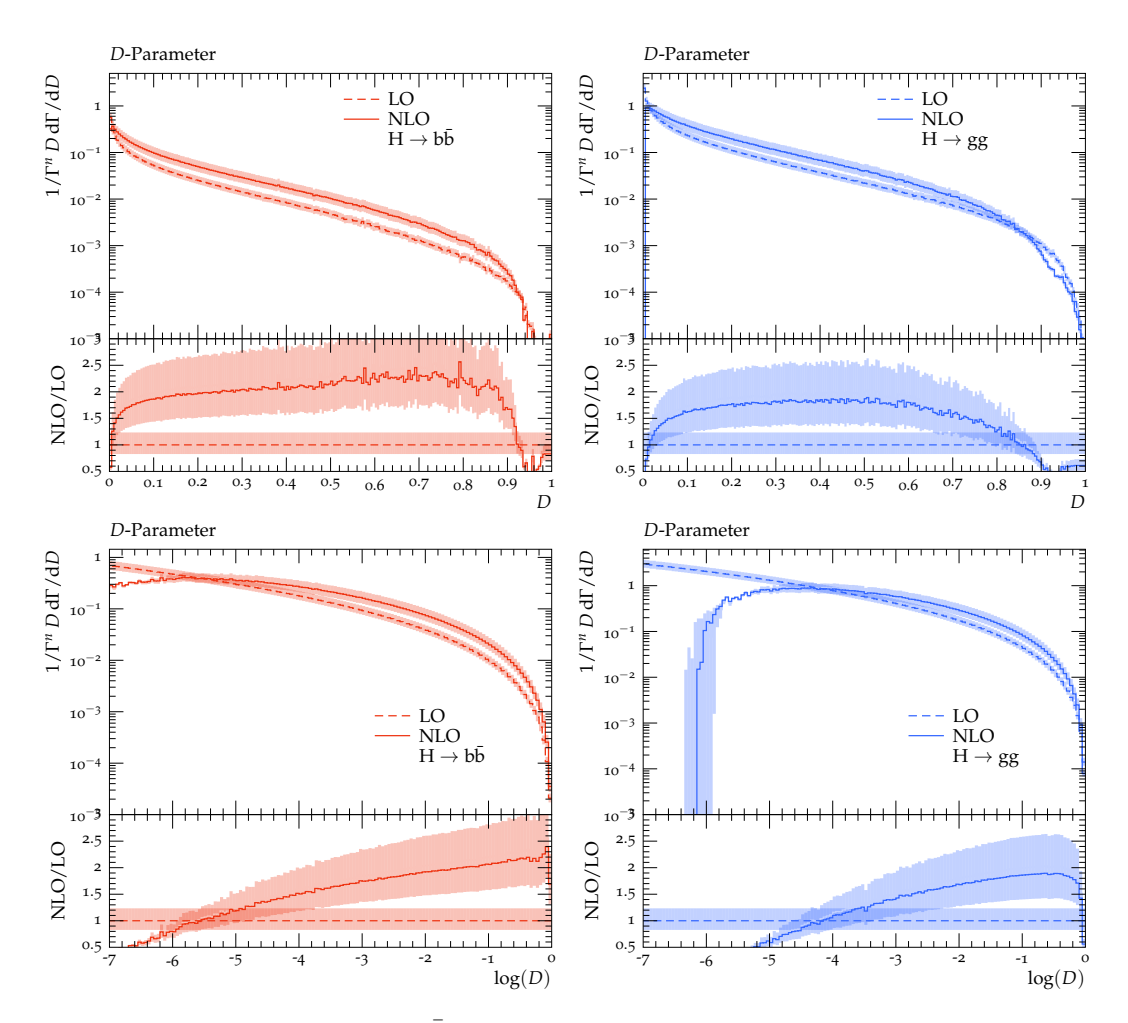


Figure 7. D-parameter in the $H \to b\bar{b}$ (*left*) and $H \to gg$ (*right*) decay category. The top row shows linearly binned histograms, the bottom row shows the same histograms with logarithmic binning, see main text.

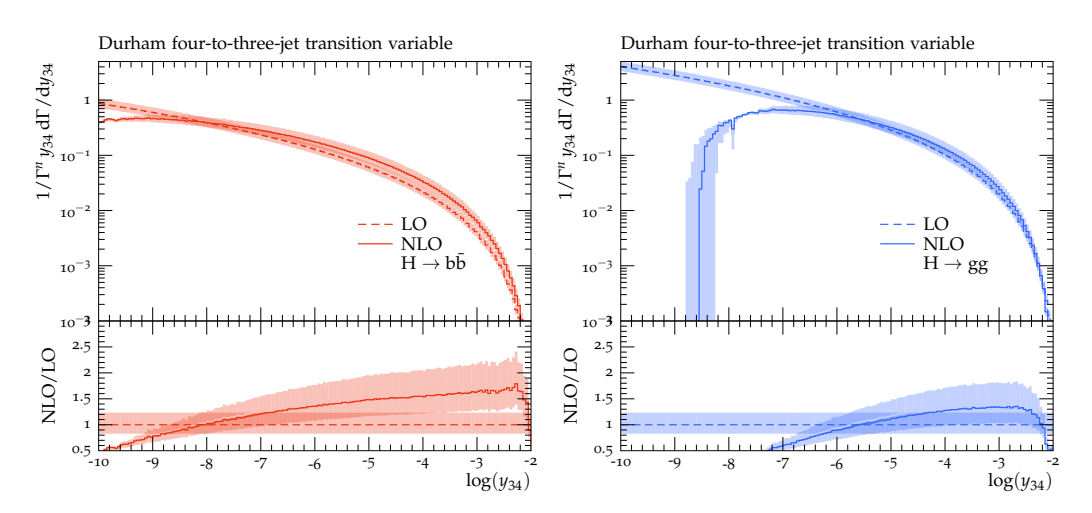


Figure 8. Durham four-to-three jet transition variable denoted by y_{34} in the H \rightarrow bb (*left*) and H \rightarrow gg (*right*) decay category, see main text.

4 Conclusions

In this paper we have, for the first time, presented results for four-jet-like event-shape observables in hadronic Higgs decays calculated including NLO corrections in perturbative QCD. Specifically, we computed the five event shapes related to the four-jet-like event shape variables thrust minor, light-hemisphere mass, narrow jet broadening, *D*-parameter and the four-to-three-jet transition variable in the Durham algorithm.

Using the antenna subtraction framework, we have implemented our computation in the existing EERAD3 parton-level Monte-Carlo generator extended to deal with hadronic Higgs decay observables, with four-parton final states at Born level.

The calculation was performed in an effective theory under the assumption of massless b-quarks with finite Yukawa coupling and an infinitely heavy top-quark, leading to the consideration of two distinct classes of processes, belonging to the Hgg and Hbb Higgs-decay categories.

We observe that all of the distributions show the characteristic behaviour of event-shape observables at fixed order in perturbative QCD. Specifically, the LO predictions diverge towards positive infinity in the infrared limit, whereas the NLO predictions develop a peak close to the limit before diverging towards negative infinity.

We have shown that all of the event shapes receive large NLO corrections with K-factors at the central scale between 1.7-2.3 in the Hb $\bar{\rm b}$ decay category and 1.3-1.8 in the Hgg decay category, depending on the observable. Interestingly, the NLO corrections are slightly smaller in H \rightarrow gg decays. This can be explained by the normalisation to the NLO two-particle decay width, which receives larger corrections in the H \rightarrow gg case and as such leads to a stronger scaling in this decay category. If, instead, a normalisation to the LO two-parton decay width was chosen, we would find larger NLO K-factors for distributions in the H \rightarrow gg category. In both decay categories, the largest NLO corrections can be observed for the D-parameter and thrust minor. The size of the NLO corrections for the narrow jet broadening, light-hemisphere mass, and the four-jet resolution is slightly smaller.

Concerning the shape of the distributions inside a given Higgs decay category, we have shown that all event-shape distributions display very similar behaviour at LO, whereas the shape visibly changes at NLO level. For all observables considered here, the shape of the NLO corrections is rather flat for Hb $\bar{\rm b}$ decays, while it is more curved in Hgg decays. We further find visible shape differences between the Yukawa-induced and gluonic decay categories at NLO. Specifically, we observe a characteristic shift of the peaks of the NLO distributions away from the infrared limit for H \rightarrow gg decays, accompanied by a similar shift of the intersection of the LO and NLO predictions.

Our calculation provides crucial ingredients for the computation of higher-order QCD corrections for event-shape observables in hadronic Higgs decays. Most imminently, it gives access to precise predictions including next-to-leading order corrections to four-jet-like event-shape observables in all hadronic Higgs-decay channels, as needed for phenomenological studies of Higgs decay properties, at a future lepton collider. While we have focussed only on decays to bottom quarks here, it is straightforward to extend our implementation to decays to other quark flavour species. We have implemented our computation in such a way that it facilitates the matching to resummed predictions in the future. Our calculation also

provides part of the real-virtual and double-real contributions to the NNLO calculation of three-jet event-shape observables. To this end, the NLO subtraction terms used here need to be suitably extended to NNLO-type subtraction terms. As we have here constructed all subtraction terms within the antenna-subtraction framework, this is a straightforward extension and will be subject of future work.

Acknowledgments

The authors are grateful to Stefano Pozzorini for helpful advices on the renormalisation schemes used in OpenLoops2. The authors also wish to thank Damien Geissbühler for his contribution to the computation of observables in the Hgg category at an early stage of this project. CTP and AG are supported by the Swiss National Science Foundation (SNF) under contract 200021-197130 and by the Swiss National Supercomputing Centre (CSCS) under project ID ETH5f. CW is supported by the National Science Foundation through awards NSF-PHY-1652066 and NSF-PHY-201402.

Open Access. This article is distributed under the terms of the Creative Commons Attribution License (CC-BY4.0), which permits any use, distribution and reproduction in any medium, provided the original author(s) and source are credited.

References

- [1] FCC collaboration, FCC-ee: The Lepton Collider. Future Circular Collider Conceptual Design Report Volume 2, Eur. Phys. J. ST 228 (2019) 261.
- [2] CEPC Study Group collaboration, CEPC Conceptual Design Report: Volume 2 Physics & Detector, arXiv:1811.10545 [INSPIRE].
- [3] ILC collaboration, The International Linear Collider Technical Design Report Volume 2: Physics, arXiv:1306.6352 [INSPIRE].
- [4] ATLAS collaboration, Observation of $H \to b\bar{b}$ decays and VH production with the ATLAS detector, Phys. Lett. B **786** (2018) 59 [arXiv:1808.08238] [INSPIRE].
- [5] CMS collaboration, Observation of Higgs boson decay to bottom quarks, Phys. Rev. Lett. 121 (2018) 121801 [arXiv:1808.08242] [INSPIRE].
- [6] G. Dissertori et al., First determination of the strong coupling constant using NNLO predictions for hadronic event shapes in e⁺e⁻ annihilations, JHEP 02 (2008) 040 [arXiv:0712.0327] [INSPIRE].
- [7] G. Dissertori et al., Determination of the strong coupling constant using matched NNLO+NLLA predictions for hadronic event shapes in e⁺e⁻ annihilations, JHEP **08** (2009) 036 [arXiv:0906.3436] [INSPIRE].
- [8] JADE collaboration, Determination of the Strong Coupling alpha(s) from hadronic Event Shapes with O(α³(s)) and resummed QCD predictions using JADE Data, Eur. Phys. J. C 64 (2009) 351 [arXiv:0810.1389] [INSPIRE].
- [9] A.H. Hoang, D.W. Kolodrubetz, V. Mateu and I.W. Stewart, Precise determination of α_s from the C-parameter distribution, Phys. Rev. D 91 (2015) 094018 [arXiv:1501.04111] [INSPIRE].

- [10] A. Verbytskyi et al., High precision determination of α_s from a global fit of jet rates, JHEP **08** (2019) 129 [arXiv:1902.08158] [INSPIRE].
- [11] A. Kardos, G. Somogyi and A. Verbytskyi, Determination of α_S beyond NNLO using event shape averages, Eur. Phys. J. C 81 (2021) 292 [arXiv:2009.00281] [INSPIRE].
- [12] A. Gehrmann-De Ridder, T. Gehrmann, E.W.N. Glover and G. Heinrich, *NNLO corrections to event shapes in* e^+e^- *annihilation*, *JHEP* **12** (2007) 094 [arXiv:0711.4711] [INSPIRE].
- [13] A. Gehrmann-De Ridder, T. Gehrmann, E.W.N. Glover and G. Heinrich, *NNLO moments of event shapes in* e^+e^- *annihilation*, *JHEP* **05** (2009) 106 [arXiv:0903.4658] [INSPIRE].
- [14] A. Gehrmann-De Ridder, T. Gehrmann, E.W.N. Glover and G. Heinrich, *EERAD3: Event shapes and jet rates in electron-positron annihilation at order* α_s^3 , *Comput. Phys. Commun.* **185** (2014) 3331 [arXiv:1402.4140] [INSPIRE].
- [15] S. Weinzierl, The infrared structure of $e^+e^- \rightarrow 3$ jets at NNLO reloaded, JHEP **07** (2009) 009 [arXiv:0904.1145] [INSPIRE].
- [16] S. Weinzierl, Event shapes and jet rates in electron-positron annihilation at NNLO, JHEP 06 (2009) 041 [arXiv:0904.1077] [INSPIRE].
- [17] S. Weinzierl, Moments of event shapes in electron-positron annihilation at NNLO, Phys. Rev. D 80 (2009) 094018 [arXiv:0909.5056] [INSPIRE].
- [18] V. Del Duca et al., Jet production in the CoLoRFulNNLO method: event shapes in electron-positron collisions, Phys. Rev. D 94 (2016) 074019 [arXiv:1606.03453] [INSPIRE].
- [19] A. Kardos, G. Somogyi and Z. Trócsányi, Soft-drop event shapes in electron-positron annihilation at next-to-next-to-leading order accuracy, Phys. Lett. B 786 (2018) 313 [arXiv:1807.11472] [INSPIRE].
- [20] T. Becher, G. Bell and M. Neubert, Factorization and Resummation for Jet Broadening, Phys. Lett. B 704 (2011) 276 [arXiv:1104.4108] [INSPIRE].
- [21] T. Becher and G. Bell, NNLL Resummation for Jet Broadening, JHEP 11 (2012) 126 [arXiv:1210.0580] [INSPIRE].
- [22] M. Balsiger, T. Becher and D.Y. Shao, NLL' resummation of jet mass, JHEP 04 (2019) 020 [arXiv:1901.09038] [INSPIRE].
- [23] A.H. Hoang, D.W. Kolodrubetz, V. Mateu and I.W. Stewart, C-parameter distribution at N³LL' including power corrections, Phys. Rev. D 91 (2015) 094017 [arXiv:1411.6633] [INSPIRE].
- [24] A. Banfi, H. McAslan, P.F. Monni and G. Zanderighi, A general method for the resummation of event-shape distributions in e⁺e⁻ annihilation, JHEP **05** (2015) 102 [arXiv:1412.2126] [INSPIRE].
- [25] A. Bhattacharya, M.D. Schwartz and X. Zhang, Sudakov shoulder resummation for thrust and heavy jet mass, Phys. Rev. D 106 (2022) 074011 [arXiv:2205.05702] [INSPIRE].
- [26] A. Bhattacharya et al., NNLL resummation of Sudakov shoulder logarithms in the heavy jet mass distribution, JHEP 11 (2023) 080 [arXiv:2306.08033] [INSPIRE].
- [27] T. Gehrmann, M. Jaquier and G. Luisoni, Hadronization effects in event shape moments, Eur. Phys. J. C 67 (2010) 57 [arXiv:0911.2422] [INSPIRE].
- [28] G. Luisoni, P.F. Monni and G.P. Salam, C-parameter hadronisation in the symmetric 3-jet limit and impact on α_s fits, Eur. Phys. J. C 81 (2021) 158 [arXiv:2012.00622] [INSPIRE].

- [29] F. Caola et al., On linear power corrections in certain collider observables, JHEP 01 (2022) 093 [arXiv:2108.08897] [INSPIRE].
- [30] F. Caola et al., Linear power corrections to e^+e^- shape variables in the three-jet region, JHEP 12 (2022) 062 [arXiv:2204.02247] [INSPIRE].
- [31] N. Agarwal et al., Next-to-leading power corrections to the event shape variables, arXiv:2306.17601 [INSPIRE].
- [32] S. Kluth, Jet physics in e^+e^- annihilation from 14-GeV to 209-GeV, Nucl. Phys. B Proc. Suppl. 133 (2004) 36 [hep-ex/0309070] [INSPIRE].
- [33] A. Signer and L.J. Dixon, Electron-positron annihilation into four jets at next-to-leading order in alpha-s, Phys. Rev. Lett. 78 (1997) 811 [hep-ph/9609460] [INSPIRE].
- [34] L.J. Dixon and A. Signer, Complete $O(\alpha_s^3)$ results for $e^+e^- \to (\gamma, Z) \to four\ jets$, Phys. Rev. D **56** (1997) 4031 [hep-ph/9706285] [INSPIRE].
- [35] G. Parisi, Super Inclusive Cross-Sections, Phys. Lett. B 74 (1978) 65 [INSPIRE].
- [36] Z. Nagy and Z. Trocsanyi, Four jet production in e⁺e⁻ annihilation at next-to-leading order, Nucl. Phys. B Proc. Suppl. **64** (1998) 63 [hep-ph/9708344] [INSPIRE].
- [37] Z. Nagy and Z. Trocsanyi, Next-to-leading order calculation of four jet shape variables, Phys. Rev. Lett. 79 (1997) 3604 [hep-ph/9707309] [INSPIRE].
- [38] Z. Nagy and Z. Trocsanyi, Next-to-leading order calculation of four jet observables in electron positron annihilation, Phys. Rev. D 59 (1999) 014020 [Erratum ibid. 62 (2000) 099902] [hep-ph/9806317] [INSPIRE].
- [39] Z. Nagy and Z. Trocsanyi, Multijet rates in e⁺e⁻ annihilation: Perturbation theory versus LEP data, Nucl. Phys. B Proc. Suppl. **74** (1999) 44 [hep-ph/9808364] [INSPIRE].
- [40] J.M. Campbell, M.A. Cullen and E.W.N. Glover, Four jet event shapes in electron-positron annihilation, Eur. Phys. J. C 9 (1999) 245 [hep-ph/9809429] [INSPIRE].
- [41] A. Banfi, G. Marchesini, Y.L. Dokshitzer and G. Zanderighi, *QCD analysis of near-to-planar three jet events*, *JHEP* **07** (2000) 002 [hep-ph/0004027] [INSPIRE].
- [42] A. Banfi, Y.L. Dokshitzer, G. Marchesini and G. Zanderighi, Near-to-planar three jet events in and beyond QCD perturbation theory, Phys. Lett. B 508 (2001) 269 [hep-ph/0010267] [INSPIRE].
- [43] A. Banfi, Y.L. Dokshitzer, G. Marchesini and G. Zanderighi, *Nonperturbative QCD analysis of near-to-planar three jet events*, *JHEP* **03** (2001) 007 [hep-ph/0101205] [INSPIRE].
- [44] A. Banfi, Y.L. Dokshitzer, G. Marchesini and G. Zanderighi, *QCD analysis of D parameter in near to planar three jet events*, *JHEP* **05** (2001) 040 [hep-ph/0104162] [INSPIRE].
- [45] A.J. Larkoski and A. Procita, New Insights on an Old Problem: Resummation of the D-parameter, JHEP 02 (2019) 104 [arXiv:1810.06563] [INSPIRE].
- [46] L. Arpino, A. Banfi and B.K. El-Menoufi, Near-to-planar three-jet events at NNLL accuracy, JHEP 07 (2020) 171 [arXiv:1912.09341] [INSPIRE].
- [47] J. Gao, Probing light-quark Yukawa couplings via hadronic event shapes at lepton colliders, JHEP 01 (2018) 038 [arXiv:1608.01746] [INSPIRE].
- [48] J. Gao, Y. Gong, W.-L. Ju and L.L. Yang, Thrust distribution in Higgs decays at the next-to-leading order and beyond, JHEP 03 (2019) 030 [arXiv:1901.02253] [INSPIRE].

- [49] M.-X. Luo, V. Shtabovenko, T.-Z. Yang and H.X. Zhu, Analytic Next-To-Leading Order Calculation of Energy-Energy Correlation in Gluon-Initiated Higgs Decays, JHEP 06 (2019) 037 [arXiv:1903.07277] [INSPIRE].
- [50] J. Gao, V. Shtabovenko and T.-Z. Yang, Energy-energy correlation in hadronic Higgs decays: analytic results and phenomenology at NLO, JHEP 02 (2021) 210 [arXiv:2012.14188] [INSPIRE].
- [51] G. Coloretti, A. Gehrmann-De Ridder and C.T. Preuss, QCD predictions for event-shape distributions in hadronic Higgs decays, JHEP 06 (2022) 009 [arXiv:2202.07333] [INSPIRE].
- [52] M. Knobbe, F. Krauss, D. Reichelt and S. Schumann, Measuring hadronic Higgs boson branching ratios at future lepton colliders, Eur. Phys. J. C 84 (2024) 83 [arXiv:2306.03682] [INSPIRE].
- [53] R. Mondini, M. Schiavi and C. Williams, N³LO predictions for the decay of the Higgs boson to bottom quarks, JHEP **06** (2019) 079 [arXiv:1904.08960] [INSPIRE].
- [54] R. Mondini and C. Williams, $H \to b\bar{b}j$ at next-to-next-to-leading order accuracy, JHEP **06** (2019) 120 [arXiv:1904.08961] [INSPIRE].
- [55] T. Inami, T. Kubota and Y. Okada, Effective Gauge Theory and the Effect of Heavy Quarks in Higgs Boson Decays, Z. Phys. C 18 (1983) 69 [INSPIRE].
- [56] A. Djouadi, J. Kalinowski and P.M. Zerwas, *Higgs radiation off top quarks in high-energy* e^+e^- colliders, Z. Phys. C **54** (1992) 255 [INSPIRE].
- [57] K.G. Chetyrkin, B.A. Kniehl and M. Steinhauser, Hadronic Higgs decay to order α_s^4 , Phys. Rev. Lett. **79** (1997) 353 [hep-ph/9705240] [INSPIRE].
- [58] K.G. Chetyrkin, B.A. Kniehl and M. Steinhauser, Decoupling relations to $O(\alpha_s^3)$ and their connection to low-energy theorems, Nucl. Phys. B **510** (1998) 61 [hep-ph/9708255] [INSPIRE].
- [59] K.G. Chetyrkin, J.H. Kuhn and C. Sturm, QCD decoupling at four loops, Nucl. Phys. B 744 (2006) 121 [hep-ph/0512060] [INSPIRE].
- [60] Y. Schroder and M. Steinhauser, Four-loop decoupling relations for the strong coupling, JHEP 01 (2006) 051 [hep-ph/0512058] [INSPIRE].
- [61] P.A. Baikov, K.G. Chetyrkin and J.H. Kühn, Five-Loop Running of the QCD coupling constant, Phys. Rev. Lett. 118 (2017) 082002 [arXiv:1606.08659] [INSPIRE].
- [62] J.A.M. Vermaseren, S.A. Larin and T. van Ritbergen, The four loop quark mass anomalous dimension and the invariant quark mass, Phys. Lett. B 405 (1997) 327 [hep-ph/9703284] [INSPIRE].
- [63] R. Mondini, U. Schubert and C. Williams, Top-induced contributions to $H \to b\bar{b}$ and $H \to c\bar{c}$ at $\mathcal{O}(\alpha_s^3)$, JHEP 12 (2020) 058 [arXiv:2006.03563] [INSPIRE].
- [64] A. Gehrmann-De Ridder, T. Gehrmann and E.W.N. Glover, Antenna subtraction at NNLO, JHEP 09 (2005) 056 [hep-ph/0505111] [INSPIRE].
- [65] J. Currie, E.W.N. Glover and S. Wells, Infrared Structure at NNLO Using Antenna Subtraction, JHEP 04 (2013) 066 [arXiv:1301.4693] [INSPIRE].
- [66] A. Gehrmann-De Ridder, T. Gehrmann, E.W.N. Glover and G. Heinrich, Jet rates in electron-positron annihilation at $O(\alpha_s^3)$ in QCD, Phys. Rev. Lett. 100 (2008) 172001 [arXiv:0802.0813] [INSPIRE].
- [67] J. Kuipers, T. Ueda, J.A.M. Vermaseren and J. Vollinga, FORM version 4.0, Comput. Phys. Commun. 184 (2013) 1453 [arXiv:1203.6543] [INSPIRE].

- [68] R. Britto, F. Cachazo, B. Feng and E. Witten, Direct proof of tree-level recursion relation in Yang-Mills theory, Phys. Rev. Lett. 94 (2005) 181602 [hep-th/0501052] [INSPIRE].
- [69] Z. Bern, L.J. Dixon, D.C. Dunbar and D.A. Kosower, One loop n point gauge theory amplitudes, unitarity and collinear limits, Nucl. Phys. B 425 (1994) 217 [hep-ph/9403226] [INSPIRE].
- [70] R. Britto, F. Cachazo and B. Feng, Generalized unitarity and one-loop amplitudes in N = 4 super-Yang-Mills, Nucl. Phys. B 725 (2005) 275 [hep-th/0412103] [INSPIRE].
- [71] D. Forde, Direct extraction of one-loop integral coefficients, Phys. Rev. D 75 (2007) 125019 [arXiv:0704.1835] [INSPIRE].
- [72] P. Mastrolia, Double-Cut of Scattering Amplitudes and Stokes' Theorem, Phys. Lett. B 678 (2009) 246 [arXiv:0905.2909] [INSPIRE].
- [73] S.D. Badger, Direct Extraction Of One Loop Rational Terms, JHEP 01 (2009) 049 [arXiv:0806.4600] [INSPIRE].
- [74] X. Chen, T. Gehrmann, E.W.N. Glover and M. Jaquier, *Precise QCD predictions for the production of Higgs + jet final states*, *Phys. Lett. B* **740** (2015) 147 [arXiv:1408.5325] [INSPIRE].
- [75] X. Chen et al., NNLO QCD corrections to Higgs boson production at large transverse momentum, JHEP 10 (2016) 066 [arXiv:1607.08817] [INSPIRE].
- [76] J.M. Campbell, R.K. Ellis and C. Williams, Hadronic Production of a Higgs Boson and Two Jets at Next-to-Leading Order, Phys. Rev. D 81 (2010) 074023 [arXiv:1001.4495] [INSPIRE].
- [77] V. Del Duca, A. Frizzo and F. Maltoni, *Higgs boson production in association with three jets*, JHEP **05** (2004) 064 [hep-ph/0404013] [INSPIRE].
- [78] S.D. Badger, E.W.N. Glover and V.V. Khoze, MHV rules for Higgs plus multi-parton amplitudes, JHEP 03 (2005) 023 [hep-th/0412275] [INSPIRE].
- [79] L.J. Dixon, E.W.N. Glover and V.V. Khoze, MHV rules for Higgs plus multi-gluon amplitudes, JHEP 12 (2004) 015 [hep-th/0411092] [INSPIRE].
- [80] R.K. Ellis, W.T. Giele and G. Zanderighi, Virtual QCD corrections to Higgs boson plus four parton processes, Phys. Rev. D 72 (2005) 054018 [Erratum ibid. 74 (2006) 079902] [hep-ph/0506196] [INSPIRE].
- [81] S.D. Badger and E.W.N. Glover, One-loop helicity amplitudes for $H \to gluons$: The All-minus configuration, Nucl. Phys. B Proc. Suppl. 160 (2006) 71 [hep-ph/0607139] [INSPIRE].
- [82] S.D. Badger, E.W.N. Glover and K. Risager, One-loop phi-MHV amplitudes using the unitarity bootstrap, JHEP 07 (2007) 066 [arXiv:0704.3914] [INSPIRE].
- [83] E.W.N. Glover, P. Mastrolia and C. Williams, One-loop phi-MHV amplitudes using the unitarity bootstrap: The General helicity case, JHEP 08 (2008) 017 [arXiv:0804.4149] [INSPIRE].
- [84] S. Badger, E.W. Nigel Glover, P. Mastrolia and C. Williams, One-loop Higgs plus four gluon amplitudes: Full analytic results, JHEP 01 (2010) 036 [arXiv:0909.4475] [INSPIRE].
- [85] L.J. Dixon and Y. Sofianatos, Analytic one-loop amplitudes for a Higgs boson plus four partons, JHEP 08 (2009) 058 [arXiv:0906.0008] [INSPIRE].
- [86] S. Badger, J.M. Campbell, R.K. Ellis and C. Williams, Analytic results for the one-loop NMHV Hqqgg amplitude, JHEP 12 (2009) 035 [arXiv:0910.4481] [INSPIRE].
- [87] J. Alwall et al., MadGraph 5: Going Beyond, JHEP 06 (2011) 128 [arXiv:1106.0522] [INSPIRE].

- [88] J. Alwall et al., The automated computation of tree-level and next-to-leading order differential cross sections, and their matching to parton shower simulations, JHEP **07** (2014) 079 [arXiv:1405.0301] [INSPIRE].
- [89] F. Buccioni et al., OpenLoops 2, Eur. Phys. J. C 79 (2019) 866 [arXiv:1907.13071] [INSPIRE].
- [90] J. Pires and E.W.N. Glover, Double real radiation corrections to gluon scattering at NNLO, Nucl. Phys. B Proc. Suppl. 205-206 (2010) 176 [arXiv:1006.1849] [INSPIRE].
- [91] E.W. Nigel Glover and J. Pires, Antenna subtraction for gluon scattering at NNLO, JHEP 06 (2010) 096 [arXiv:1003.2824] [INSPIRE].
- [92] R. Kleiss, W.J. Stirling and S.D. Ellis, A New Monte Carlo Treatment of Multiparticle Phase Space at High-energies, Comput. Phys. Commun. 40 (1986) 359 [INSPIRE].
- [93] Particle Data Group collaboration, Review of Particle Physics, PTEP **2022** (2022) 083C01 [INSPIRE].
- [94] S. Brandt, C. Peyrou, R. Sosnowski and A. Wroblewski, *The Principal axis of jets. An Attempt to analyze high-energy collisions as two-body processes*, *Phys. Lett.* **12** (1964) 57 [INSPIRE].
- [95] E. Farhi, A QCD Test for Jets, Phys. Rev. Lett. 39 (1977) 1587 [INSPIRE].
- [96] L. Clavelli, Jet Invariant Mass in Quantum Chromodynamics, Phys. Lett. B 85 (1979) 111 [INSPIRE].
- [97] S. Catani, G. Turnock and B.R. Webber, Jet broadening measures in e⁺e⁻ annihilation, Phys. Lett. B 295 (1992) 269 [INSPIRE].